Potential for landsliding: Dependence on hyetograph characteristics

Paolo D'Odorico
Department of Environmental Sciences, University of Virginia, Charlottesville, Virginia, USA

Sergio Fagherazzi
Department of Geological Sciences and School of Computational Science and Information Technology, Florida State University, Tallahassee, Florida, USA

Riccardo Rigon
Dipartimento di Ingegneria Civile e Ambientale, Universitá di Trento/CUDAM, Trento, Italy

Received 27 January 2004; revised 8 November 2004; accepted 14 December 2004; published 10 February 2005.

[1] This paper examines the effect of hyetograph shape on the potential for landsliding in soil-mantled landscapes. An existing pore pressure response model (Iverson, 2000) is used to study the effects of unsteady rainfall infiltration in hillslopes, and the effect of slope and convergent topography is expressed using a steady state model of slope-parallel subsurface flow. Slope stability is assessed using an infinite slope analysis. This theoretical framework is coupled with simple hyetograph models and to intensity-duration-frequency functions to determine the return period of landslide-triggering rainfall. Results also show that hyetographs with a peak at the end of a rainfall event have a stronger destabilizing effect than hyetographs with a constant rainfall or with a peak at the beginning of a storm. Thus the variability of hyetograph shapes adds uncertainty to the assessment of landsliding triggered by rainfall.

Citation: D'Odorico, P., S. Fagherazzi, and R. Rigon (2005), Potential for landsliding: Dependence on hyetograph characteristics, *J. Geophys. Res.*, *110*, F01007, doi:10.1029/2004JF000127.

1. Introduction

[2] The stability of hillslopes and hollows is affected by extreme rainfalls which increase the soil water pressure and consequently reduce the shear strength of the aggregates, favoring the instability of the soil mantle. The triggering of landslides by rainfall has been studied on different slopes, bedrock substrates, soil depths and ages, and with different vegetation [*O'Loughlin and Pearce*, 1976; *Sidle and Swanston*, 1982; *Reneau and Dietrich*, 1987; *Trustrum and De Rose*, 1988; *Montgomery et al.*, 1998; *Iida*, 1999; *Wieczorek et al.*, 2000; *Morrissey et al.*, 2001]. The process-based assessment of whether a slope is stable or unstable is important to landslide hazard assessment, mapping of landslide-prone areas [*Montgomery and Dietrich*, 1994; *Dietrich et al.*, 1995; *Iida*, 1999], and studies of landform evolution [e.g., *Benda and Dunne*, 1997a, 1997b; *D'Odorico and Fagherazzi*, 2003], as well as to investigations of the dependence of landslide frequency on soil mechanical properties, land cover, and topography [e.g., *Sidle and Swanston*, 1982; *Sidle*, 1987; *Iida*, 1999].

[3] This paper puts together an existing body of modeling approaches and hydrological concepts in a methodology to calculate the return period of landslide-triggering precipitation. In particular, we explore (1) the relationship existing between landslide occurrence and the intensity, duration, and frequency of precipitation (through the IDF curves expressed as power laws [e.g., *Koutsoyiannis and Foufoula-Georgiou*, 1993; *Burlando and Rosso*, 1996]); (2) the relative importance of long-term (slope-parallel) flow with respect to short-term (vertical) infiltration in the triggering of landslides; and (3) the influence of the shape of the storm hyetographs on the return period of landslide-triggering precipitation.

[4] We assume that the pressure head transient observable in the course of a rainstorm is due to the unsteady vertical flow through the soil profile, while slope-parallel subsurface flow is assumed to occur at a longer timescale and to determine the prestorm wetness conditions. We therefore couple a model of subsurface lateral (steady) flow [*Montgomery and Dietrich*, 1994; *Iida*, 1999] with a model of transient rainfall infiltration [*Iverson*, 2000] to determine the hydrologic conditions that cause slope failure. The return period of these hydrologic conditions is determined through the intensity-duration-frequency relations of extreme precipitation. Moreover, simplified models of the complex temporal structure of storm hyetographs are used here to study the effect of hyetograph shape on slope stability.

2. Spatial and Temporal Variability of Soil Water Pressure

[5] Rainfall infiltration in soil-mantled hillslopes is characterized by different scales: the subhorizontal hillslope scale, from the divide to the stream, is generally of the order of hundreds of meters, whereas soil thickness is

0148-0227/05/2004JF000127$09.00

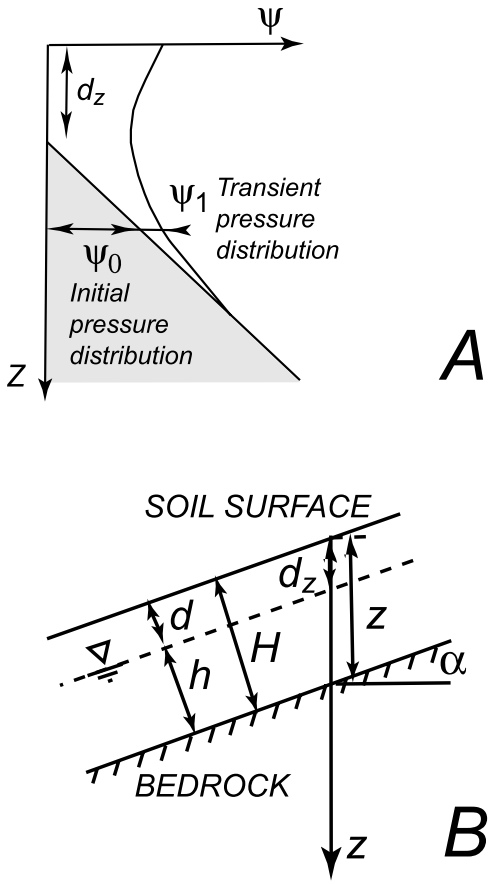

Figure 1. (a) Steady state and transient distribution of pressure head in the soil column. (b) Schematic of the slope.

usually of the order of a few meters or less. Thus the slope-parallel unsaturated flow occurs at a timescale longer than infiltration, and its effect on water pressure variability can be negligible at the storm timescale with respect to vertical infiltration. However, topography-controlled subsurface flow affects the long-term moisture patterns within the basin and determines the pressure head, ψ_0, attained in the interstorm period prior to the beginning of the storm. Thus the pressure head of water within the soil column can be expressed as a sum of two components [*Iverson*, 2000], $\psi = \psi_0 + \psi_1$ (Figure 1a): ψ_0, produced by the long-term infiltration rate I_{steady}, and ψ_1, the short-term response to rainstorms.

2.1. Long-Term Piezometric Conditions

[6] In the case of slope-parallel subsurface flow, the long-term piezometric response linearly increases with the vertical saturated depth ($Z - d_z$) (Figure 1a) [*Iverson*, 1990, 2000]:

$$\psi_0 = (Z - d_z)\ \cos^2\alpha, \tag{1}$$

where d_z is the depth of the water table at the beginning of the storm (Figures 1a and 1b) and α the slope angle. The average long-term subsurface flow in interflow periods is thus controlled by hillslope topography. The spatial variability of ψ_0 can be determined by using steady state, topography-based models [*Beven and Kirkby*, 1979; *Montgomery and Dietrich*, 1994]. The long-term wetness ratio, W, defined as the ratio between saturated depth, h, and the thickness of the soil column, H (Figure 1b), can be expressed [*Montgomery and Dietrich*, 1994] as

$$W = \frac{h}{H} = \frac{q\,A}{b\,T\,\sin\alpha}, \tag{2}$$

where q is the net (long-term) rainfall rate, A is the contributing area, b is the slope width, T is the transmissivity ($T = KH$, where K is the saturated hydraulic conductivity and is assumed to be constant through the soil profile [*Montgomery and Dietrich*, 1994]). Thus since $(d_z/Z) = (d/H) = 1 - W$ (see Figure 1b), equation (1) can be rewritten as

$$\psi_0 = W\,Z\cos^2\alpha, \tag{3}$$

where W depends only on the slope topography, the hydraulic conductivity and the long-term net precipitation. The topographic index $A/(b\sin\alpha)$ has been used [*Montgomery and Dietrich*, 1994] as an indicator of the geomorphic factors controlling landslide occurrence in soil-mantled landscapes. Maps of this index can be used to detect landslide-prone areas in a watershed.

2.2. Short-Term Pressure Head Response to Precipitation

[7] The short-term piezometric response, ψ_1, to intense rainfall events of rate, I_z was determined by *Iverson* [2000] through a linearized version of *Richards* [1931] equation. This approach is based on the assumption that when the soil water content is close to saturation, the hydraulic conductivity, K, and the soil water capacity, C, can be considered to be constant, although this is valid only for small variations in soil saturation [*Hillel*, 1998]. The solution of the linearized Richards equations with suitable initial and boundary conditions provides the distribution of groundwater pressure head as a function of time [*Iverson*, 2000]. Combining *Iverson* [2000] solution for ψ_1 with (3), the following expression is obtained for the soil water pressure distribution:

$$\frac{\psi(t^*)}{Z} = \begin{cases} W\cos^2\alpha + \dfrac{I_z}{K_z}[R(t^*)] & 0 \le t^* \le T^* \\ W\cos^2\alpha + \dfrac{I_z}{K_z}[R(t^*) - R(t^* - T^*)] & t^* \ge T^* \end{cases}, \tag{4}$$

where the second addendum on the right hand side of equation (4) represents the time-dependent component of the (normalized) soil water pressure and will be indicated as ψ_1^*, while R is the response function [*Iverson*, 2000]:

$$R(t^*) = \sqrt{t^*/\pi}\exp(-1/t^*) - erfc\left(1/\sqrt{t^*}\right). \tag{5}$$

In equations (4) and (5), t^* is the nondimensional time, and T^* is the nondimensional rainfall duration:

$$t^* = \frac{t}{T_D}, T^* = \frac{T}{T_D}, T_D = \frac{Z^2}{D}, \tag{6}$$

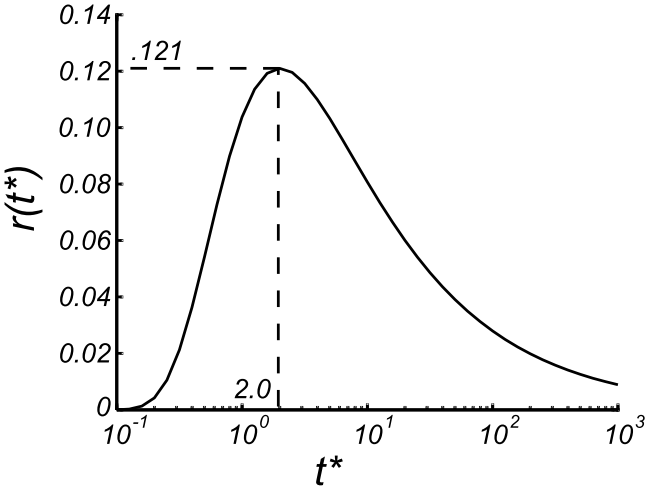

Figure 2. Instantaneous response function.

where T is the storm duration and D is a diffusion coefficient, which depends on slope angle, α, saturated hydraulic conductivity, K_{sat}, and water capacity at saturation, C_0, which, in a saturated soil, results from changes in porosity caused by changes in pressure head [e.g., *Bear*, 1972]:

$$D = \frac{4D_0}{\cos^2\alpha} = 4\frac{K_{\text{sat}}}{C_0\cos^2\alpha}. \tag{7}$$

Iverson's solution is based on the simplified framework of linear diffusion; however, it has been argued that the nonlinearities associated with the state dependence of unsaturated hydraulic conductivity and water capacity can play an important role in the hillslope response to precipitation [*Montgomery and Dietrich*, 2002]. Macroporosity and preferential flow through fractured bedrocks add further complexity to the water pressure regime within the soil [*Montgomery et al.*, 2002]. All these factors are not accounted for by equation (4). A more realistic framework should incorporate soil heterogeneities leading to preferential flow, since pore pressure can be dominated by the effects of vertical flow in macropores (e.g., tension cracks, decayed roots, or subsurface erosion channels) [*Beven and Germann*, 1982; *Sidle et al.*, 1995]. Small variations in soil hydraulic properties may also influence slope instability, causing locally elevated pore water pressures with a destabilizing effect [*Reid and Iverson*, 1992; *Reid*, 1997]. However, given the limited availability of distributed data on soil macropores, we simply assume that the effective (saturated) hydraulic conductivity is increased to account for the presence of macropores. More sophisticated models, utilizing for example a dual porosity framework [*Gerke and van Genuchten*, 1993], are of difficult application without extensive field measurements.

3. Dependence on the Hyetograph Characteristics

3.1. Case of Uniform Hyetographs

[8] The simplest model of hyetograph is with constant rainfall intensity throughout individual rainstorms:

$$I^*(t^*) = \bar{I}^* H(T^* - t^*), \tag{8}$$

where $\bar{I}^* = \bar{I}/K$ (with $\bar{I}$ being the constant rainfall rate), H is the Heaviside's step function (i.e., $H(T^* - t^*) = 1$, if $0 < T^* - t^* < 1$; $H(T^* - t^*) = 0$, otherwise). In particular, in the study of hillslope stability it is important to refer to the peak values of pressure head at different depths. The peak time, t_p^*, is determined by solving the condition $d\psi^*/dt^* = 0$ using equation (4):

$$\begin{aligned} &\bar{I}^*\frac{dR(t^*)}{d}t^* = \bar{I}^* r(t^*) = 0 && (0 \le t^* \le T^*) \\ &\bar{I}^*\frac{dR(t^*)}{dt^*} = \bar{I}^*(r(t^*) - r(t^* - T^*)) = 0 && t^* \ge T^*, \end{aligned} \tag{9}$$

with

$$r(t^*) = \frac{dR(t^*)}{dt^*} = \frac{1}{2\sqrt{\pi\, t^*}}\exp\left(-\frac{1}{t^*}\right). \tag{10}$$

The first of equations (9) is never satisfied because $r(t^*)$ is always larger than zero (equation (10)). Hence pressure reaches its peak value at a time, t_p, subsequent to the end of the rainstorm, such that $r(t_p^*) - r(t_p^* - T^*) = 0$. This is partly supported by field experiments showing that the pressure head at the soil/bedrock interface never decreases during irrigation intervals in a steep unchanneled catchment [*Torres et al.*, 1998] (Figure 2). Notice from equation (9) how the peak time is independent of precipitation intensity and return period.

[9] Equation (9) can be (numerically) solved providing the estimation of t_p^*, for different values of rainfall duration, T^*, as shown in Figure 3a. It is possible to observe that t_p^* is almost constant for $T^* < 1$, while it linearly increases with T^* when $T^* > 1$. In fact, for small durations ($T^* < 1$), the pressure head response tends to the instantaneous response function, $r(t)$, and the pressure head peak occurs after a time interval equal to $2T_D$ (see equation (6)). For longer rainfall durations the pressure head peak occurs for $t_p^* = T^*$, hence at the end of the rainfall event. The pressure head $\psi(t)$ depends both on the duration, T, and on the return period, T_r, of the extreme events. This dependence can be expressed through the intensity-duration-frequency (IDF) curves characterizing the regime of extreme precipitation in the region under question. The IDF function is often expressed as [e.g., *Koutsoyiannis and Foufoula-Georgiou*, 1993; *Burlando and Rosso*, 1996; *Kottegoda and Rosso*, 1997, p. 471]

$$I_Z(T, T_r) = a(T_r)T^{-m} \quad \text{or} \quad I^* = a^*(T_r)T^{*-m}, \tag{11}$$

with a^* being equal to $a(T_r)D^m/(K_z\, Z^{2m})$ and $I^* = I_z/K$. In equation (11) the dependence on the return period could be expressed only through the parameters a (or a^*) and m. However, it is easy to show that m has to be independent of T_r. In fact, for a given return period the plot on logarithmic axes of intensity as a function of duration is a straight line (equation (11)) with slope m. Intensity-duration plots associated with different return periods need to have the same slope (i.e., the same m) otherwise they would intersect and (within a certain interval of rainfall durations) the intensity of (extreme) precipitation would be lower with the higher return period. Thus in equation (11) only a (or a^*) depends on T_r. The relation between the depth, $D_z = T\, I_z$,

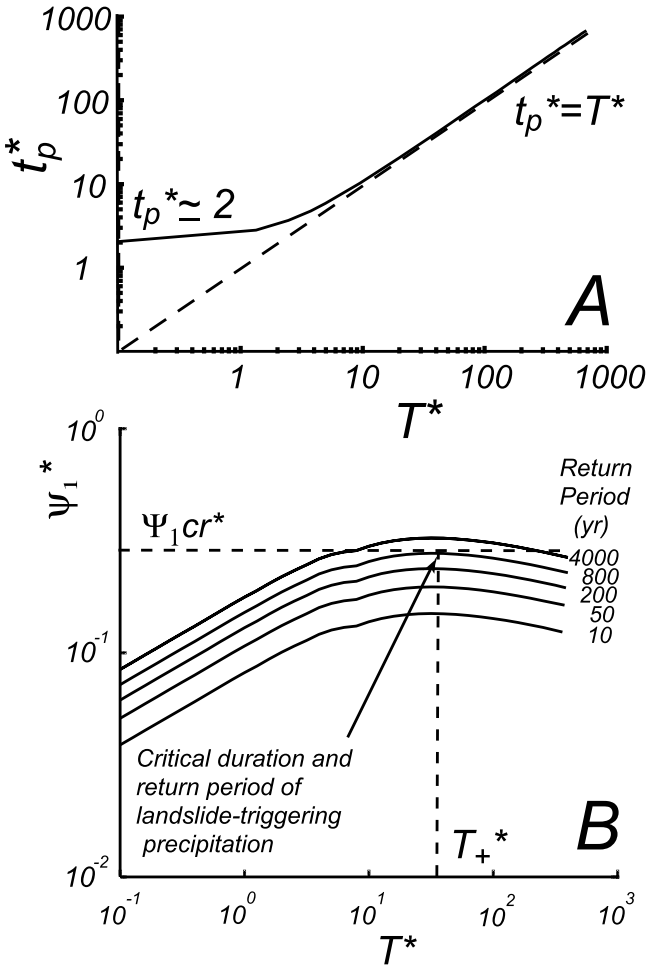

Figure 3. (a) Normalized peak time as a function of the normalized rainstorm duration, which corresponds to equation (13) (modified from *Iverson* [2000, Figure 6]). (b) Plot of pressure head ψ_1^* versus normalized rainfall duration T^* for different return periods. The curve tangent to the line $\psi_1^* = \psi_{1cr}^*$ (with ψ_{1cr}^* being the minimum pressure head able to trigger a landslide on that slope) gives the critical duration and the return period, T_+^*, of landslide-triggering rainfall. The data refer to the hollow W41 in Table 2.

and the duration of (extreme) precipitation can be obtained from equation (11), $D_z = a\ T^{1-m}$. Because the storm depth is an increasing function of the duration, the exponent, $1 - m$, needs to be positive (i.e., $m < 1$). At the same time, m needs to be positive because I_z, decreases with T. Thus m is expected to range between 0 and 1, and is commonly found to be between 0.5 and 1 [*Wenzel*, 1982].

[10] Through the use of the IDF curves it is possible to estimate the return period of landslide-triggering precipitation. For any given value of the return period there exists a critical rainfall duration, T_+^*, associated with maximum peak values of soil water pressure. On the other hand, rainfall events of duration T_+^* generate peak values of water pressure which increase with increasing values of the return period (Figure 3b). The return period of the triggering precipitation is found as the return period of rainstorms with duration T_+^* and peak water pressure, ψ_{cr}^* (calculated with (12) for $T^* = T_+^*$), that are critical to slope stability, as shown in Figure 3b. This condition theoretically determines the lowest return period (as well as the intensity and duration) of rainstorms able to trigger a landslide.

[11] Equation (11) in (4) can be used to determine the rainfall duration, T_+^*, producing maximum values of soil water pressure at the peak time, t_p^*. In fact, the peak pressure, $\psi(t_p^*)$, can be expressed as a function of T^* by calculating (4) at the peak time and expressing the dependence of t_p^* on T^* (Figure 3a):

$$\psi_p^*(T^*) = W\cos^2\alpha + a^*(T_r)T^{*-m} \cdot \left[R\left(t_p^*(T^*)\right) - R\left(t_p^*(T^*) - T^*\right)\right], \tag{12}$$

where $\psi^* = \psi/Z$.

[12] Notice how $a^*(T_r)T^{*-m}$ is a decreasing function of T^*, while the term between square brackets decreases with increasing values of T^*. The value, T_+^* of T^* maximizing the peak pressure, ψ_p^*, can be determined by setting at zero the first derivative of (12) with respect to T^*:

$$-m\left[R\left(t_p^*(T^*)\right) - R\left(t_p^*(T^*) - T^*\right)\right] + T^*\left(r\left(t_p^*(T^*)\right)\frac{dt_p^*}{dT^*} - r\left(t_p{}^*(T^*) - T^*\right)\frac{dt_p{}^*}{dT^*} + r\left(t_p^*(T^*) - T^*\right)\right) = 0. \tag{13}$$

Equation (13) is independent of the return period, T_r, of the event; thus, the rainfall duration, T_+^*, affecting (for a given return period) slope stability in the most severe manner depends only on the hillslope geotechnical and hydrologic conditions as well as on the type of relationship existing between intensity and duration of (extreme) precipitation (i.e., the parameter m). Once the critical rainfall duration, T_+^*, has been determined through (13), equation (11) can be utilized to calculate rainfall intensity as a function of the return period. Equation (13) can be numerically solved for different values of m: the results of this analysis are shown in Figure 4a. Figure 4b shows the peak value of the (normalized) transient pressure head, ψ_1^*/a^*, as a function of rainfall duration for different values of the parameter m: ψ_1^*/a^* is independent of the return period and has its maximum at $T^* > 1$.

[13] Figure 4a gives a synthetic expression of the hydraulic, hydrologic and geomechanic conditions affecting the stability of a natural slope. In fact, given the soil thickness and the hydraulic parameters it is possible to determine the critical rainfall duration as a function of the parameter m of the IDF function (equation (11)). The maximum peak value of pressure head, $\psi_{\max}^*$, is then calculated using equation (12) with $T^* = T_+^*$. The stability conditions can be then assessed by estimating the safety factors, FS, for different values of the return period [e.g., *Terzaghi and Peck*, 1967; *Iverson*, 1991]:

$$\mathrm{FS} = \frac{\tan\phi}{\tan\alpha} + \frac{c}{\gamma_s Z\ \sin\alpha\ \cos\alpha} - \frac{\psi\ \gamma_w\ \tan\phi}{\gamma_s Z \sin\alpha\ \cos\alpha}, \tag{14}$$

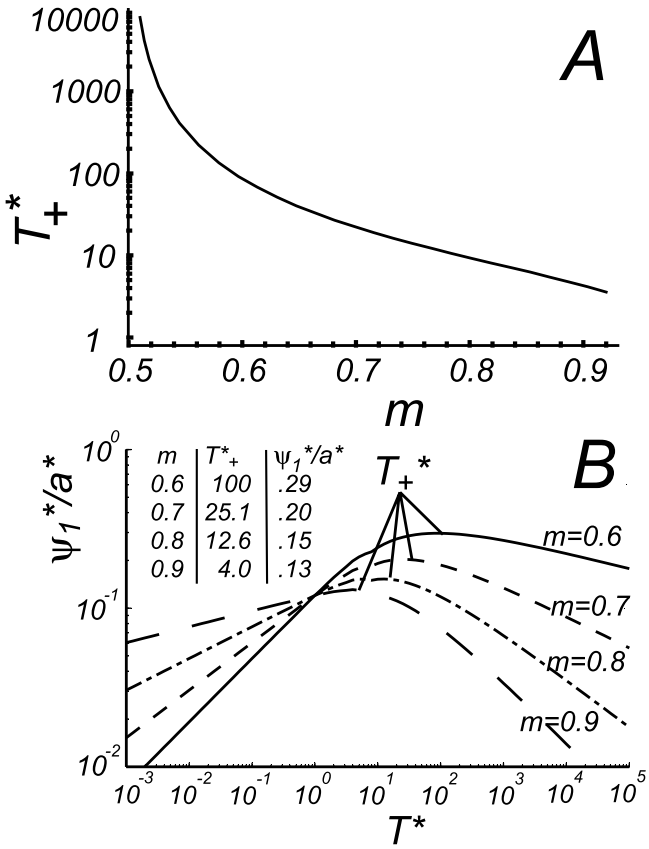

Figure 4. (a) Duration of the critical precipitation as a function of the parameter m of the intensity-duration-frequency (IDF) curves. (b) Plot of normalized transient pressure head ψ_1^*/a^* (independent of return period) versus normalized rainfall duration T^* for different values of m. The peak is always for $T^* > 1$. The table in the inset shows maximum values of ψ_1^*/a^* corresponding to different values of m (i.e., different climatic conditions).

with ϕ being the angle of internal friction, α the slope angle, c the cohesion, γ_s and γ_w the specific weight of (bulk) soil and water, respectively. Possible applications of this analysis include the estimation of the lowest return period associated with the emergence of unstable conditions, as well as the estimation of the landsliding potential. For example, the determination of the return period of landslide-triggering precipitation can be carried out as follows: (1) the depth of the failure surface is assigned; (2) given the soil morphological and hydrological characteristics, the critical value of the pressure head, ψ_p^*, at the specified depth is determined by solving for ψ equation (14) with FS = 1; (3) the critical rainfall duration, T_+^*, is calculated with (13), and as noticed before, T_+^* is independent of the return period; (4) the return period of landsliding is computed through (12), utilizing the calculated values of ψ_p^* and T^*; and (5) the value of the critical rainfall intensity is finally calculated from (11) once the return period is known. The procedure can be repeated at different soil depths thus determining the return period of both shallow and deep landslides. This is important because short and intense events can induce elevated pore pressures and create instability at shallow depths, whereas longer and less intense rainfalls may affect the hillslope stability to greater depths [*Iverson*, 2000]. The lowest return period will then indicate the soil depth at which failure is more likely to occur.

3.2. Case of Nonuniform Hyetographs

[14] In the previous section the intensity of precipitation is assumed to be constant throughout a rainstorm. However, the temporal structure of rainfall is more complex. It is possible to extend this framework to the case of nonuniform hyetographs, to assess how significant is the dependence on the hyetograph structure. A number of theoretical hyetograph models developed for other hydrologic applications can be applied also to slope stability analyses. Models of single-peak hyetographs [e.g., *Chow et al.*, 1988] have been followed by stochastic models able to represent both the temporal variability and the randomness of precipitation [e.g., *Garcia-Guzman and Aranda-Oliver*, 1993], as well as its scaling properties [e.g., *Koutsoyiannis and Foufoula-Georgiou*, 1993]. Instead of focusing on the determination of a hyetograph model able to provide the best representation of extreme rainstorms in a specific region, hyetographs are here modeled in a rather general manner as β functions:

$$I^*(t^*) = \bar{I}^*\beta\left(\frac{t^*}{T^*}\right)H(T^* - t^*), \tag{15}$$

where

$$\beta\left(\frac{t^*}{T^*}\right) = \frac{\Gamma(p)}{\Gamma(q)\,\Gamma(p-q)}\left(\frac{t^*}{T^*}\right)^{q-1}\left(1 - \frac{t^*}{T^*}\right)^{p-q-1}. \tag{16}$$

In (15), H is the Heaviside's step function, while $\bar{I}^*$ is the rainstorm average intensity. $\bar{I}^*$ can be expressed as a function of rainfall duration and return period through the IDF function (11). More details on the mathematical properties of the β function (equation (16)) can be found by *Benjamin and Cornell* [1970, pp. 287–290]. The hyetograph (15) has different shapes depending on the parameters p and q (Figure 5). Thus this model is able to represent a variety of rainstorm structures (except for multiple-peak hyetographs) and is here used to single out which of them is able to cause landslides more easily.

[15] The linearization [*Iverson*, 2000] of the *Richards* [1931] equation allows us to express the piezometric response to storm (15) using the instantaneous response function, $r(t^*)$ (equation (10)), in conjunction with the convolution integral

$$\psi^* = W\cos^2\alpha + \int_0^{t^*} I^*(\tau)r(t^* - \tau)d\tau. \tag{17}$$

The dependence between the peak time of soil water pressure, t_p^*, and the storm duration, T^*, can be determined by setting to zero the derivative of equation (17) with respect to t^*. The convolution integral (17) together with the r function defined in (10) allow analysis of continuously varying precipitation intensity, thus improving the theoretical formulation of *Iverson* [2000] in which only a discretely varying precipitation intensity can be represented in rainfall histograms.

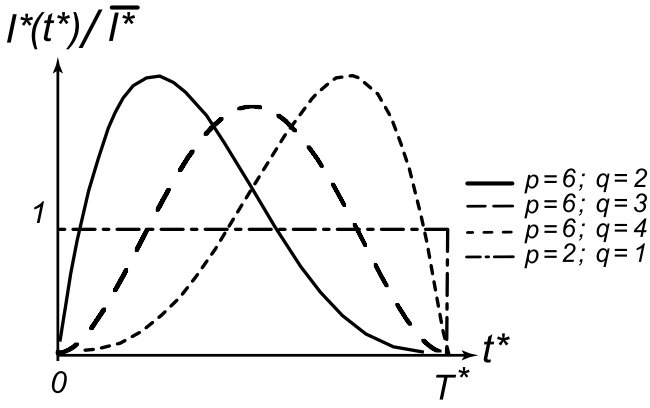

Figure 5. Representation of the storm hyetographs by means of β functions.

[16] The results of this analysis are shown in Figure 6a: the relationship between t_p^* and T^* is independent of the return period and is significantly affected by the shape of the hyetograph. In particular, the peak value of soil water pressure occurs before the end of the event, except for the case of rainstorms having relatively short durations. Moreover the peak time is larger when the center of mass of the hyetograph is closer to the end of the event.

[17] The duration, T_+^*, of the event associated with highest peak values of soil water pressure has been determined as a function of m (Figure 6b). The values of T_+^* are independent of the return period and significantly vary with the exponent m of the IDF function as well as with the shape of the hyetograph. The effect of hyetograph shape on the peak values of transient soil water pressure, ψ_1^*, has been assessed by calculating the values of ψ_1^*/a^* for $T^* = T_+^*$ and $t^* = t_p^*(T_+^*)$. The results of this analysis are shown in Figure 6c. It is possible to observe that the use of uniform hyetographs leads to soil water pressures that are about 20–25% less than in the case of a hyetograph with the same rainfall volume, but with a peak near to the end of the storm. This fact leads to the conclusion that the use of constant rainfall intensity, for a given rainfall depth, underestimates the likelihood of landslide occurrence.

[18] These results can be used to calculate the return period of precipitation able to trigger a landslide on a slope of given topography, soil mechanical properties, thickness, and preexisting moisture conditions: (1) combining equations (1), (2), and (14), the minimum value of ψ_1^* able to trigger a landslide can be determined from the condition FS = 1 as

$$\psi_1^* = \frac{\gamma_s}{\gamma_w}\left(1 - \frac{\tan\alpha}{\tan\phi}\right)\cos^2\alpha - W\cos^2\alpha + \frac{c}{\gamma_\omega Z \tan\phi}; \quad (18)$$

(2) given the exponent, m, of the IDF function (calculated from rainfall records) the critical value of ψ_1^*/a^* is determined from Figure 6c; (3) the combination of 1 and 2 gives the critical value of a^*. The return period, T_r, associated with a^* is finally calculated.

4. A Case Study

[19] As an application of this framework we consider a small area on the Appalachian Mountains (Madison County, Virginia), southeast of Shenandoah National Park. This region can be affected by intense rainstorms in the course of the summer and fall months. In particular, on 27 June 1995, 330–750 mm of rain fell within a period of 16 hours;

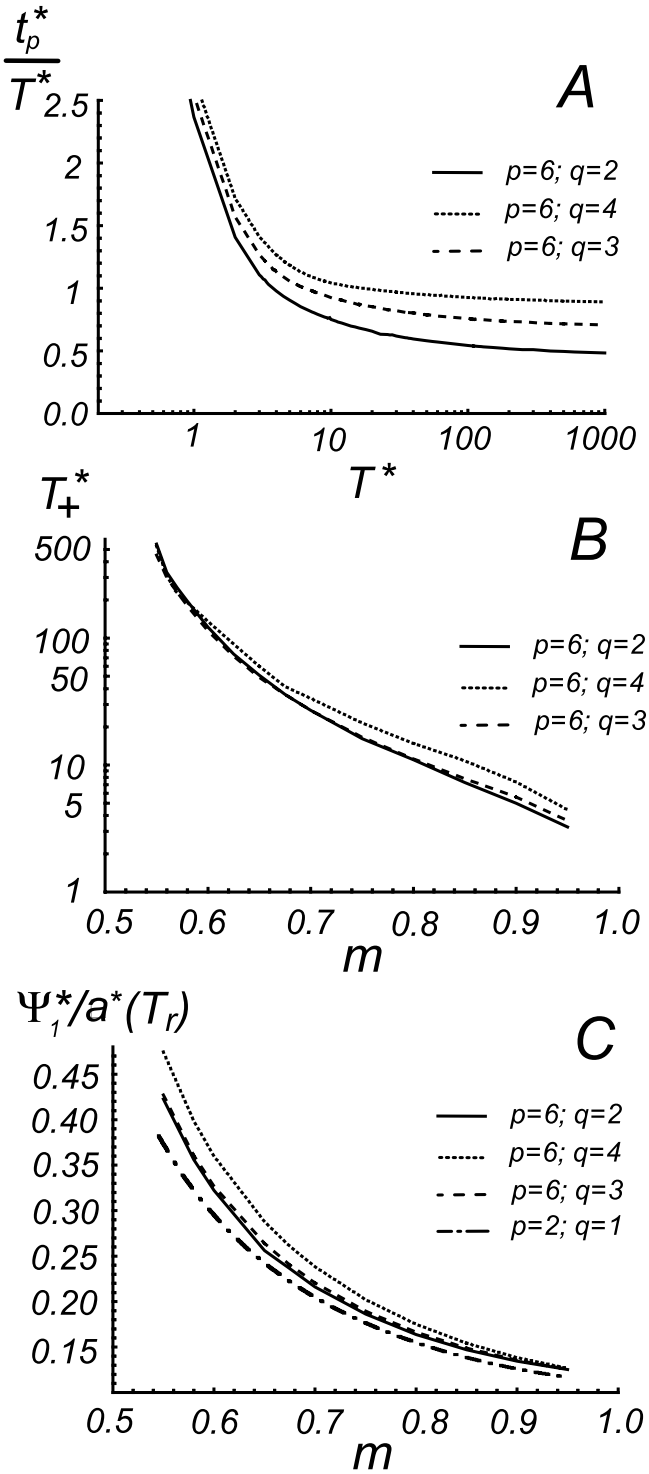

Figure 6. (a) Normalized peak time as a function of storm duration. (b) Duration of the critical precipitation as a function of the m parameter of the IDF curves and of the shape of the hyetograph. (c) Maximum water pressure excess, ψ_1^*, as a function of the m parameter and of the shape of the hyetograph.

Table 1. Values of the Parameters Determined by *Morrissey et al.* [2001] for the Hollows in Madison County, Virginia

Parameter	Value
Slope angle (α), deg	17–41
Angle of internal friction (φ), deg	25
Soil cohesion (c), kPa	4.0
Soil specific weight (γ_s), kN m^{-3}	11.8
Saturation hydraulic conductivity (K_z), m s^{-1}	10^{-5}
Hydraulic diffusivity (D_0), m^2 s^{-1}	10^{-3}
Water table depth (d)	same as Z

this precipitation triggered more than 600 debris flows in an area of about 130 km^2 [*Wieczorek et al.*, 2000; *Morrissey et al.*, 2001]. The storm was preceded by 75–170 mm of rain in the previous five days, leading to antecedent moisture conditions with water table close to the ground surface [*Smith et al.*, 1996]. Most of the landslides had thickness of 0.5–3.0 m and occurred on slopes ranging between 17° and 41° [*Morrissey et al.*, 2001].

[20] *Morrissey et al.* [2001] applied *Iverson*'s [2000] model to assess the stability of these slopes; they determined the soil geotechnical and hydrologic parameters (Table 1) characteristic of this area in Madison County. The soil cohesion was assumed to be low ($C \sim 4$ kPa), as the root-soil system was found to be above the failure plane.

[21] The framework developed in this paper can be used to analyze the stability of the hollows surveyed by *Morgan et al.* [1997] in Madison County, Virginia. The parameters will be assumed to be the same as determined by *Morrissey et al.* [2001]. The analysis of the IDF curves for this region gives $m = 0.675$ and $a = 65.67$ mm h^{m-1}, $a = 72.44$ mm h^{m-1}, $a = 80.72$ mm h^{m-1}, with return periods of 25, 50, and 100 years, respectively. This analysis is based on values reported in the rainfall frequency atlas of the eastern United States (National Weather Service, http://www.erh.noaa.gov/er/hq/Tp40s.htm). The debris flow source areas considered in this study were surveyed by *Morgan et al.* [1997] and their characteristics are reported in Table 2. In the application of our model we locate the failure plane at a depth corresponding to the landslide scar depth measured in the field by *Morgan et al.* [1997]. The contributing areas were calculated using 10 m × 10 m DEMs, and were used, along with the other topographic parameters (Table 2), to calculate the preexisting conditions expressed by the long-term wetness ratio, W (equation (2)). W depends on the average rate, q_r, of net precipitation contributing to the long-term soil moisture conditions of the hillslope. The estimation of q_r is not an easy task: it depends on the average rainfall rate, on the evaporation losses due to canopy and litter interception, and on transpiration losses of water that is locally uptaken by vegetation [e.g., *Ridolfi et al.*, 2003]. The average total annual precipitation measured in this area (Big Meadow, Virginia, 1936–1997) is 1229 mm, which corresponds to an average

Table 2. Characteristics of the Landslides Considered in This Study[a]

ID #	Elevation, m	α, deg	H, cm	b, m	A, m^2	$A/[bH\sin(\alpha)]$, $\times 10^4$	T_r*, years	T_r**, years
W-20	588.26	34	200	11.60	1400	0.0108	546	141
W-22a	594.36	30	30	5.20	2400	0.3092	14	6
W-23	536.45	30	200	11.30	2600	0.0230	733	181
W-40	670.56	30	100	10.70	10100	0.1889	38	15
W-41	536.45	23	350	38.10	42000	0.0807	824	199
W	499.87	28	380	36.60	49100	0.0752	60	22
W-104	518.16	38	90	7.60	128600	3.0573	49	18
O-17	582.17	20	100	55.00	18000	0.0958	136	43
O-26	905.26	28	200	13.00	1300	0.0107	1482	329
O-43	490.73	28	100	6.00	25100	0.8915	31	13
O-45	472.44	27	100	12.00	26000	0.4776	31	13
O-68	743.71	35	100	5.80	2300	0.0692	152	48
O-69	783.34	36	100	7.60	3200	0.0717	154	48
O-70	624.84	30	50	5.50	9300	0.6766	25	10
M-59	573.02	30	100	6.00	6300	0.2101	31	13
M-89	481.58	30	200	6.10	2700	0.0443	405	109
M-90	451.10	31	100	7.00	1200	0.0333	208	62
M-109	472.44	31	200	14.00	6100	0.0423	364	99
M-110	396.24	32	100	10.00	2600	0.0491	177	54
M-111	374.90	29	100	20.00	3000	0.0310	215	64
M-117	396.24	32	300	5.00	19100	0.2404	1	1
M-118	396.24	28	100	6.00	41800	1.4846	31	13
M-139	438.91	31	200	12.00	2800	0.0227	626	158
M-150	679.70	29	200	13.00	2600	0.0206	933	222
M-151	621.79	30	100	7.00	800	0.0229	233	68
M-152	609.60	31	100	13.00	600	0.0090	271	77
M-169	548.64	30	60	19.50	29500	0.5041	29	12
M-171	652.27	40	90	6.10	2000	0.0568	217	64
G-11	585.22	35	50	7.01	5600	0.2787	35	14
G-12	487.68	35	100	9.76	5600	0.1001	110	36
G-14	499.87	35	100	8.84	1500	0.0296	231	68
G-24	463.30	27	200	7.62	4100	0.0593	450	119

[a]The first five columns report ID numbers, elevations, slope angles, debris flow thickness, and width of debris flow source areas surveyed by *Morgan et al.* [1997]. Contributing areas, A, were determined using 10 m × 10 m digital elevation models (U.S. Geological Survey). The last two columns show estimates of the return period of triggering precipitation calculated with $q_r = 1.5$ mm/d in the case of a rectangular hyetograph (*) and of a hyetograph modeled as a generalized beta function (equation (20)), with $p = 6$ and $q = 4$). We also note that according to our slope stability model, the hollow M117 is unconditionally unstable so that the return period of the triggering precipitation is 1.

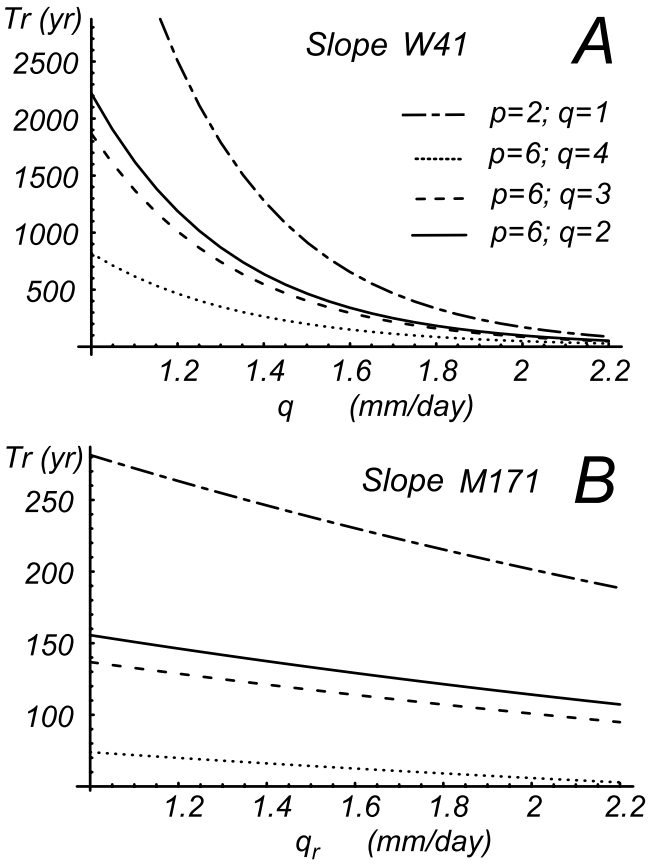

Figure 7. Return period of the triggering precipitation as a function of the "net precipitation," q_r, for (a) hollow W41 and (b) hollow M171. The return period was calculated using different hyetograph models: rectangular (bold line) and equation (20) with $p = 6$ and $q = 2$ (solid line), $p = 6$ and $q = 3$ (dashed line), and $p = 6$ and $q = 4$ (dotted line).

daily precipitation of 3.4 mm/d. July is on average the most rainy month, with an average precipitation of 4.2 mm/d. Using a runoff ratio of 0.35–0.50 for these upland portions of the watershed, q_r is found to range between 1.2 and 1.7 mm/day in the case of annual averages or between 1.5 and 2.1 for the July average precipitation.

[22] The return period, T_r, of the triggering precipitation depends on W, which, in turn, is a function of q_r. An example of this dependence is shown in Figure 7 for two different debris flow source areas: slope W41, which is fairly large (A = 42,000 m^2) and gentle (α = 23°), and slope M171, which is relatively small (A = 2000 m^2) and steep (α = 40°). The return period was calculated with different parameters of the hyetograph model (equation (16)). This analysis shows that the return period of the triggering precipitation strongly depends on the shape of the hyetograph, which represents a further source of uncertainty in the analysis of landslide potential, in addition to soil strength parameters, hillslope hydrological processes, and preexisting moisture conditions. The dramatic effect of the latters on return period estimates is also shown in Figure 7. According to this modeling framework the hillslope (or hollow) area would affect the long-term soil moisture conditions (i.e., the index W), while the unsteady flow resulting as a direct response to a rainstorm event would depend on the local slope but not on the contributing area. The influence of the long-term subsurface flow is stronger for hollows having large drainage areas, in which the convergence of slope-parallel subsurface flow can significantly affect the stability conditions. Conversely, in small and steep hollows the water pressure excess produced by vertical infiltration is the main cause of slope instability, with a dramatic influence of hyetograph shape on landslide return period (Figure 7). The overall effect of the geomorphic features of hillslopes and hollows emerges from the comparison of the results for slope W41 and M171: despite the relatively large value of W resulting from large contributing areas and small slope angles, the hollow W41 (Figure 7a) has high return periods compared to the smaller and steeper slope M171 (Figure 7b). This is due to the effect of the slope angle on the stability conditions (equation (15)). Overall higher values of W are associated with lower return periods, hence with higher likelihood of landslide occurrence, as indicated by Figure 8. W was able to explain about 40–45% of the variability of T_r in a set of 32 hollows (Table 2) sampled from the published inventory of debris flow source areas [*Morgan et al.*, 1997]. These values of the return period are reported in Table 2 for two different hyetograph shapes.

5. Discussion and Conclusions

[23] The mechanistic modeling of landslide occurrence requires both a geotechnical model of slope stability and a hydrological analysis of rainfall infiltration and subsurface flow. Several models [e.g., *Montgomery and Dietrich*, 1994; *Dietrich et al.*, 1995] assume the existence of uniform and steady subsurface flow in the shallow soil and express the soil water content as a function of a topographic index, without accounting for the dependence on rainfall duration. Because the return period of precipitation depends both on storm intensity and duration, this approach does not allow for the assessment of the likelihood of rainfall sufficient to trigger landslides. Other models account for the transient character of rainfall infiltration [*Wu and Sidle*, 1995; *Benda and Dunne*, 1997a; *Casadei et al.*, 2003; *Gabet and Dunne*,

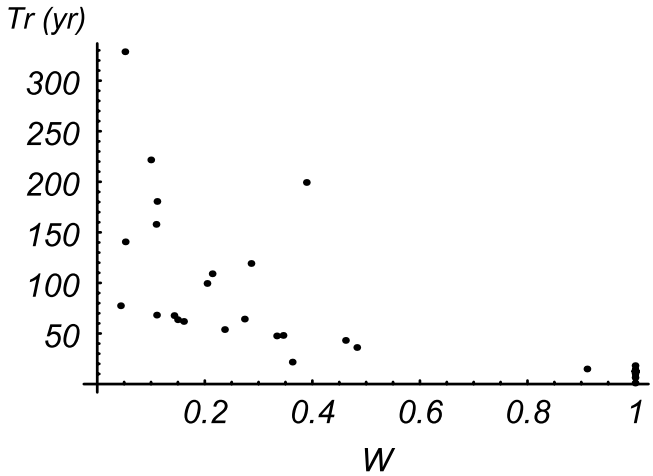

Figure 8. Return period of the triggering precipitation versus the wetness ratio, W.

2003] but lack of an explicit dependence on the characteristics of rainfall extremes (i.e., IDF relations). The approach by *Iida* [2004] accounts for this dependence within a simplified conceptual model of unsteady subsurface flow with no explicit representation of vertical infiltration through the soil column. The intensity and duration of rainfalls triggering landslides have already been studied by other authors [*Caine*, 1980; *Cannon and Ellen*, 1985; *Keefer et al.*, 1987; *Wieczorek*, 1987; *Wieczorek et al.*, 2000]. Their approach consisted in reporting on a rainfall intensity plot all the events that produced landslides in a certain geographic area. The corresponding envelope curve would represent the critical rainfall threshold for landslides and can be utilized for real-time landslide warning. However, due to the lack of a process-based analysis, this method is unable to assess the stability of a particular slope with respect to certain storm characteristics and it does not predict the return period of the landslide-triggering precipitation.

[24] Our process-based approach differs from these empirical studies because it provides the return period of the triggering precipitation. In our model the short-term hillslope response to precipitation is analyzed through a linearization [*Iverson*, 2000] of the *Richards* [1931] equation. *Iverson*'s [2000] theoretical framework is modified as follows: (1) the long-term hydrologic conditions are expressed as a function of hillslope geomorphic and hydraulic features; (2) the IDF functions are introduced as a mean to calculate the return period of landslide-triggering precipitation; and (3) the instantaneous response function, $r(t^*)$, is utilized in conjunction with a convolution integral to calculate the hillslope response to nonuniform continuous hyetographs. This approach is used to examine the effect of hyetograph shape on slope stability.

[25] The results show that (1) the duration of the most critical rainstorm is independent of the return period but is a function of the soil mechanical and hydraulic properties as well as of the exponent m of the IDF function and (2) the shape of the hyetograph affects the values of the pressure head and, consequently, the stability conditions of the hillslope. For a given rainfall depth, hyetographs with a peak near to the end of the storm produce peak pressure heads higher than uniform hyetographs, thus decreasing the return period of rainfall events causing landsliding. (3) The long-term saturated subsurface flow, which determines the depth of the water table at the beginning of the rainfall event, influences landslide frequency more in hollows with large contributing areas. In fact the convergence of subsurface flow allows for relatively high long-term pressure heads, which dominate the pressure distribution even in the course of a rainstorm. Conversely, in small and steep hollows, the excess in pressure head produced by rainfall infiltration plays a major role in determining the return period of landslides. Finally, the application of this framework to a landslide event in Virginia shows how the duration and frequency of landslide-triggering rainstorms strongly depends on the shape of the storm hyetograph as well as on the antecedent moisture conditions.

[26] **Acknowledgments.** The authors gratefully acknowledge Gerald F. Wieczorek (U.S. Geological Survey) for providing debris flow data from Madison County (VA), Emanuele Cordano for his comments and suggestions, and Christian Tiso (University of Trento) for his assistance in the use and analysis of the digital topographic data. This research was partly funded by project ASI 175/02.

References

Bear, J. (1972), *Dynamics of Fluids in Porous Media*, Dover, Mineola, N. Y.

Benda, L., and T. Dunne (1997a), Stochastic forcing of sediment supply to channel networks from landsliding and debris flow, *Water Resour. Res.*, *33*, 2849–2863.

Benda, L., and T. Dunne (1997b), Stochastic forcing of sediment routing and storage in channel networks, *Water Resour. Res.*, *33*, 2865–2880.

Benjamin, J. R., and C. A. Cornell (1970), *Probability, Statistics, and Decision for Civil Engineers*, McGraw-Hill, New York.

Beven, K., and P. Germann (1982), Macropores and water-flow in soils, *Water Resour. Res.*, *18*, 1311–1325.

Beven, K. J., and M. J. Kirkby (1979), A physically based, variable contributing area model of basin hydrology, *Hydrol. Sci. Bull.*, *24*, 43–69.

Burlando, P., and R. Rosso (1996), Scaling and multiscaling models of depth-duration-frequency curves for storm precipitation, *J. Hydrol.*, *187*, 45–64.

Caine, N. (1980), The rainfall intensity-duration control of shallow landslides and debris flows, *Geogr. Ann. A*, *62*, 23–27.

Cannon, S. H., and S. D. Ellen (1985), Rainfall conditions for abundant debris avalanches in the San Francisco Bay region, California, *California Geol.*, *38*, 267–272.

Casadei, M., W. E. Dietrich, and N. L. Miller (2003), Testing a model for predicting the timing and location of shallow landslide initiation in soil-mantled landscapes, *Earth Surf. Processes Landforms*, *28*, 925–950.

Chow, V. T., D. R. Maidment, and L. W. Mays (1988), *Applied Hydrology*, McGraw-Hill, New York.

Dietrich, W. E., R. Reiss, M. L. Hsu, and D. Montgomery (1995), A process-based model for colluvial soil depth and shallow landslides using digital elevation data, *Hydrol. Processes*, *9*, 383–400.

D'Odorico, P., and S. Fagherazzi (2003), A probabilistic model of rainfall-triggered shallow landslides in hollows: A long-term analysis, *Water Resour. Res.*, *39*(9), 1262, doi:10.1029/2002WR001595.

Gabet, E. J., and T. Dunne (2003), A stochastic sediment delivery model for a steep Mediterranean landscape, *Water Resour. Res.*, *39*(9), 1237, doi:10.1029/2003WR002341.

Garcia-Guzman, A., and E. Aranda-Oliver (1993), A stochastic model of dimensionless hyetograph, *Water Resour. Res.*, *29*, 2363–2370.

Gerke, H. H., and M. T. van Genuchten (1993), A dual-porosity model for simulating the preferential movement of water and solutes in structured porous media, *Water Resour. Res.*, *29*, 305–319.

Hillel, D. (1998), *Environmental Soil Physics: Fundamentals, Applications, and Environmental Considerations*, Elsevier, New York.

Iida, T. (1999), A stochastic hydro-geomorphological model for shallow landsliding due to rainstorm, *Catena*, *34*, 293–313.

Iida, T. (2004), Theoretical research on the relationship between return period of rainfall and shallow landslides, *Hydrol. Processes*, *18*, 739–756.

Iverson, R. M. (1990), Groundwater flow fields in infinite slopes, *Geotechnique*, *40*, 139–143.

Iverson, R. M. (1991), Sensitivity of stability analyses to groundwater data, in *Proceedings of the Sixth International Symposium on Landslides, Christchurch, New Zealand*, edited by D. H. Bell, pp. 451–457, A. A. Balkema, Brookfield, Vt.

Iverson, R. M. (2000), Landslide triggering by rain infiltration, *Water Resour. Res.*, *36*, 1897–1910.

Keefer, D. K., R. C. Wilson, R. K. Mark, E. E. Brabb, W. M. Brown III, S. D. Ellen, E. L. Harp, G. F. Wieczorek, C. S. Alger, and R. S. Zatkin (1987), Real time landslide warning during heavy rainfall, *Science*, *238*, 921–925.

Kottegoda, N. T., and R. Rosso (1997), *Probability, Statistics, and Reliability for Civil and Environmental Engineers*, McGraw-Hill, New York.

Koutsoyiannis, D., and E. Foufoula-Georgiou (1993), A scaling model of a storm hyetograph, *Water Resour. Res.*, *29*, 2345–2361.

Montgomery, D. R., and W. E. Dietrich (1994), A physically based model for the topographic control on shallow landsliding, *Water Resour. Res.*, *30*, 1153–1171.

Montgomery, D. R., and W. E. Dietrich (2002), Runoff generation in a steep, soil-mantled landscape, *Water Resour. Res.*, *38*(9), 1168, doi:10.1029/2001WR000822.

Montgomery, D. R., K. Sullivan, and H. M. Greenberg (1998), Regional test of a model for shallow landsliding, *Hydrol. Processes*, *12*, 943–955.

Montgomery, D. R., W. Dietrich, and J. T. Heffner (2002), Piezometric response in shallow bedrock at CB1: Implications for runoff generation and landsliding, *Water Resour. Res.*, *38*(10), 1274, doi:10.1029/2002WR001429.

Morgan, B. A., G. F. Wieczorek, R. H. Campbell, and P. L. Gori (1997), Debris-flow hazards in areas affected by the June 27, 1995 storm in Madison County, Virginia, *U.S. Geol. Surv. Open File Rep., 97-438*, 15 pp.

Morrissey, M. M., G. F. Wieczorek, and B. A. Morgan (2001), A comparative analysis of hazard models for predicting debris flows in Madison County, Virginia, *U.S. Geol. Surv. Open File Rep., 01-0067*, 15 pp.

O'Loughlin, C. L., and A. J. Pearce (1976), Influence of Cenozoic geology on mass movement and sediment yield response to forest removal, North Westland, New Zealand, *Bull. Int. Assoc. Eng. Geol.*, *14*, 41–46.

Reid, M. E. (1997), Slope instability caused by small variations in hydraulic conductivity, *J. Geotech. Geoenviron.*, *123*, 717–725.

Reid, M. E., and R. M. Iverson (1992), Gravity-driven groundwater flow and slope failure potential: 2. Effects of slope morphology, material properties, and hydraulic heterogeneity, *Water Resour. Res.*, *28*, 939–950.

Reneau, S. L., and W. E. Dietrich (1987), Size and location of colluvial landslides in a steep forested landscape, *IAHS Publ.*, *165*, 39–48.

Richards, L. A. (1931), Capillary conduction of liquids through porous medium, *Physics*, *1*, 318–333.

Ridolfi, L., P. D'Odorico, A. Porporato, and I. Rodriguez-Iturbe (2003), Stochastic soil moisture dynamics along a hillslope, *J. Hydrol.*, *272*, 264–275.

Sidle, R. C. (1987), A dynamic model of slope stability in zero-order basins, *IAHS Publ.*, *165*, 101–110.

Sidle, R. C., and D. N. Swanston (1982), Analysis of a small debris slide in coastal Alaska, *Can. Geotech. J.*, *19*, 167–174.

Sidle, R. C., H. Kitahara, T. Terajima, and Y. Nakai (1995), Experimental studies on the effects of pipeflow on throughflow partitioning, *J. Hydrol.*, *165*, 207–219.

Smith, J. A., M. L. Baeck, M. Steiner, and A. J. Miller (1996), Catastrophic rainfall from an upslope thunderstorm in the central Appalachians: The Rapidan storm of June 27, 1995, *Water Resour. Res.*, *32*, 3099–3113.

Terzaghi, K., and R. B. Peck (1967), *Soil Mechanics in Engineering Practice*, 729 pp., John Wiley, Hoboken, N. J.

Torres, R., W. E. Dietrich, D. R. Montgomery, S. P. Anderson, and K. Loague (1998), Unsaturated zone processes and the hydrologic response of a steep, unchanneled catchment, *Water Resour. Res.*, *34*, 1865–1879.

Trustrum, N. A., and R. C. De Rose (1988), Soil depth-age relationship of landslides on deforested hillslopes, Taranaki, New Zealand, *Geomorphology*, *1*, 143–160.

Wenzel, H. G., Jr. (1982), Rainfall for urban stormwater design, in *Urban Stormwater Hydrology*, *Water Resour. Monogr. Ser.*, vol. 7, edited by D. F. Kibler, pp. 35–67, AGU, Washington, D. C.

Wieczorek, G. F. (1987), Effect of rainfall intensity and duration on debris flows in central Santa Cruz Mountains, California, in *Debris Flows, Avalanches: Process, Recognition, and Mitigation*, *Rev. Eng. Geol.*, vol. 7, edited by J. E. Costa and G. F. Wieczorek, pp. 21–31, Geol. Soc. of Am., Boulder, Colo.

Wieczorek, G. F., B. A. Morgan, and R. H. Campbell (2000), Debris-flow hazards in the Blue Ridge of central Virginia, *Environ. Eng. Geol.*, *6*, 3–23.

Wu, W., and R. C. Sidle (1995), A distributed slope stability model for steep forested basins, *Water Resour. Res.*, *31*, 2097–2110.

P. D'Odorico, Department of Environmental Sciences, University of Virginia, 291 McCormick Road, Box 400123, Charlottesville, VA 22904-4123, USA. (paolo@virginia.edu)

S. Fagherazzi, Department of Geological Sciences, Florida State University, Tallahassee, FL 32306-4120, USA. (sergio@csit.fsu.edu)

R. Rigon, Dipartimento di Ingegneria Civile e Ambientale, Universitá di Trento/CUDAM, Mesiano di Povo, I-38100 Trento, Italy. (riccardo.rigon@ing.unitn.it)